Proceedings of ERAD (2004): 474–480 © Copernicus GmbH 2004

ERAD 2004

A radar observation operator for high-resolution non-hydrostatic numerical weather prevision

O. Caumont[1], V. Ducrocq[1], G. Delrieu[2], M. Gosset[2], J. Parent du Châtelet[3], J.-P. Pinty[4], H. Andrieu[5], Y. Lemaître[6], and G. Scialom[6]

[1]GAME/CNRM (Météo-France, CNRS), Météo-France, Toulouse, France
[2]LTHE, Grenoble, France
[3]DSO, Météo-France, Trappes, France
[4]Laboratoire d'Aérologie, Toulouse, France
[5]LCPC, Bouguenais, France
[6]CETP, Vélizy, France

Abstract. In order to specify an observation operator for radar reflectivities for the next numerical weather prediction model of Météo-France, a radar simulator was implemented in the research model Meso-NH. This tool was made up of building blocks that each describe a particular physical process (scattering, beam bending, etc.). Sensitivity experiments were carried out using different configurations for the modules. They allowed to specify an observation operator as a compromise between accuracy and computing constraints.

1 Introduction

Currently, operational Numerical Weather Prediction (NWP) systems consist of global atmospheric models which run typically at horizontal resolution ranging from 20 to 50 km and of mesoscale limited area models with about 10-km grid meshes. An important evolution in NWP systems is planned for the end of the decade: It is envisaged to replace or complement the current operational models by a new atmospheric model generation, which will be non-hydrostatic with horizontal resolution of 1 to 3 km. Almost all Eumetnet Short Range Numerical Weather Prediction (SRNWP) consortia (HIRLAM, COSMO, ALADIN, ALADIN-LACE, and UKMO) envisage such developments.

For the next generation of high-resolution models, a significant improvement of the representation of clouds and precipitation is expected, both by explicit treatment of moist convection and advanced parameterization of microphysical processes. Such improvements have already been demonstrated on some case studies, with non-hydrostatic research models like Meso-NH or MM5. These studies have also shown the necessity to improve data assimilation systems, focusing on the use of higher resolution observations, such as mesonet in situ observations or high-resolution remote sensing information like METEOSAT Second Generation (MSG) radiances or radar data. For example, the European COST-717 action aims at promoting the use of radar data in NWP and hydrological models (Alberoni et al., 2003). Indeed, ground-based radar data have the considerable advantage of having a high spatial and temporal resolution, covering large areas at different heights, and being already produced on a routine basis with increasing quality in many countries.

Météo-France, within the ALADIN consortium, has started to develop a high-resolution model, called AROME, foreseen to become operational by 2008. AROME will be designed to run at a resolution of only a few kilometers. It is planned to assimilate radar data in AROME. The French continental operational radar network, called ARAMIS, provides a good coverage with 18 C- or S-band radars, and is planned to be extended to 24 by 2006.

Since the AROME model is currently under development, it has been chosen to develop an observation operator for the research anelastic non-hydrostatic high-resolution Meso-NH model (Lafore et al., 1998), and afterwards to transfer it to the AROME software. Meso-NH allows to run simultaneously several nested grids in a two way fashion (Clark and Farley, 1984; Stein et al., 2000). A bulk microphysical scheme (Caniaux et al., 1994; Pinty and Jabouille, 1998) governs the equations of six water species: water vapour, cloud water, rainwater, primary ice, graupel, and snow. This scheme, which is representative of those that will be used for future high-resolution operational models, is going to be included in AROME.

Many radar simulators are available in the literature, but they often focus on a few specific points. Some of them concentrate on microphysics and aim at establishing relationships with their associated errors between radar measurements and the hydrometeor content of the sounded atmosphere (e.g. Vivekanandan et al., 1993). Others favor hydrological aspects (e.g. Giuli et al., 1994; Anagnostou and Krajewski, 1997; Capsoni et al., 2001; Pellarin et al., 2002; Boudevillain and Andrieu, 2003). Some attempts were made to assimilate reflectivities in high-resolution models (Wu et al., 2000), but they often included Doppler velocities only

Correspondence to: O. Caumont
(olivier.caumont@meteo.fr)

(Xiao et al., 2003; Lindskog et al., 2004). Moreover the geometrical part of the observation operators for radar Doppler velocities and reflectivities is often rough: for instance Lindskog et al. (2004) do not take beam broadening into account. It is worth being noted that Haase and Crewell (2000) have developed a complete radar reflectivity simulator named RSM (radar simulation model) that uses predicted fields of the nonhydrostatic mesoscale Lokal-Modell (LM). However, we found that some aspects deserved more attention, as their sensitivity study only examined beam bending and attenuation by air. Moreover, beam broadening was also not taken into account in RSM.

The main objective of this work is to specify an observation operator for radar reflectivities in AROME. The method consists in building a modular radar simulator in Meso-NH and carry out sensitivity tests so as to find a compromise between numerical accuracy and efficiency for the radar operator.

First, in Sect. 2, the radar simulator is described. Sect. 3 describes the Meso-NH simulation of an extreme flash-flood event that occurred on 8–9 September 2002. This case study serves as a basis for simulations of radar reflectivities and allows comparisons to observations. Last, sensitivity experiments performed on this case study provide the opportunity to specify the observation operator (Sect. 4).

2 Radar simulator

The radar simulator model is made of relatively independent modules, each one describing a particular physical process. The following subsections describe module configurations that were developed and tested in the radar simulator.

2.1 Beam shape

In order to correctly simulate the data retrieval, one has to know which volume contributes to the returned signal. This radar resolution volume is radially determined by the sampling process, and orthoradially defined by the antenna's radiation pattern.

Radar measurements consist in sampling return echoes at regular times. The power measured for each sample is used to compute corresponding reflectivities by means of the so-called radar equation, and the time delay between the emission of the pulse and the current sampling gives the range to the target. By setting the gate length to a sufficiently small value compared to the horizontal model resolution, it is not expected that the effects related to the finite receiver bandwidth (Doviak and Zrnić, 1993) will lead to significant errors. Therefore, the gate length is set to $c\tau/2$ (c is the celerity of light in vacuum, and τ is the pulse time width), and we assume that all scatterers located in this gate equally contribute to the received signal.

The easiest way to model the antenna's radiation pattern is to represent the transmitted wave as isotropically spherical within a well-determined solid angle. But this approximation gives unsatisfactory results. Probert-Jones (1962) modeled the antenna's directivity pattern as a Gaussian function. Assuming that the cone of resolution is sufficiently small so that hydrometeor properties can be kept constant within it, he derived a formula for reflectivities close to the isotropic case, but only multiplied by a corrective factor. One can further refine this approach by considering changes in hydrometeor properties within the resolution cone. In our simulator, this is numerically done by means of Gauss-Hermite or Gauss-Legendre quadrature. It is to be noted that using one point in Gauss-Hermite quadrature yields the same results as initially proposed by Probert-Jones (1962): a constant directivity function within a cone of revolution, multiplied by a corrective factor. With this method, it is unrealistic to take more than about three points because the integration interval spans over a too wide range. Therefore the Gauss-Hermite quadrature cannot match the model resolution in the lower atmosphere. With the Gauss-Legendre quadrature, the integration interval is fixed — we set it to the -3 dB level angle. All points used by this quadrature method lie within this interval, and increasing their number results in increasing the resolution of the quadrature method. One can therefore adapt the number of points so as to match the model resolution. However, with this method, it is necessary to use at least several points to obtain accurate results. This method is consequently ill-adapted for low resolution integrations.

2.2 Beam bending

As it travels through the atmosphere, the radar beam encounters different refractive indices. This variation is responsible for the bending of the electromagnetic beam according to Snell's law. At radio frequencies, the refractive index n is mainly influenced by water vapor partial pressure, total pressure, and temperature. From experimental datasets, Smith and Weintraub (1953) drew the following relationship:

$$N = \frac{77.6}{T}\left(p + 4810\frac{e}{T}\right), \quad (1)$$

where $N = (n-1)\times 10^6$ is the refractivity, p is the total pressure (hPa), e is the water vapor partial pressure (hPa), and T is the temperature (K). It is thence possible to compute the path of the radar ray. However this method is computationally expensive and requires a good knowledge of the atmosphere state especially at low levels. For most situations, however, it is satisfactory to use an effective Earth's radius (Schelleng et al., 1933). Assuming an Earth slightly larger than the real one, the propagation path would be a straight line. This actually corresponds to an idealized atmosphere, which enables straightforward analytical computation of each radar gate height. This idealized atmosphere model simply states that the refractive index vertical gradient is equal to $-1/(4a)$, where a is the Earth's radius. In this case, the effective Earth's radius is $4/3$ larger than the real one. In a few situations, the actual refractive index vertical gradient will substantially differ from $-1/(4a)$. The issue is critical when the vertical gradient is lower than the adopted

value, for low elevations, because this can result in the beam hitting the ground.

2.3 Scattering processes

Equivalent reflectivity factors (z_e, in m^3) are computed by evaluating the following equation

$$z_e(\mathbf{r}) = \frac{\lambda^4 l^2(\mathbf{r})}{\pi^5 |K_w|^2} \sum_{j \in \text{type}} \int_0^\infty \sigma_j(D) N_j(D, \mathbf{r}) \, \mathrm{d}D \,, \qquad (2)$$

where $\mathbf{r}$ denotes the vector the origin of which is the radar antenna that designates the current gate, λ (in m) is the wavelength of the radar pulse, K_w is the dielectric factor of water (usually 0.93), the j subscript refers to each hydrometeor type, σ (in m^2) is the backscattering cross-section of a particle of diameter D (in m), N_j (in m^{-4}) is the size distribution of the j^{th} type of hydrometeor, and $l^2(\mathbf{r})$ is the total two-path attenuation which can be written as

$$l^2(\mathbf{r}) = \exp\left(-2 \int_0^r \sum_{j \in \text{type}} \int_0^\infty C_{ej}(D) N_j(D, \mathbf{r}) \, \mathrm{d}D \, \mathrm{d}r\right) , \qquad (3)$$

where C_{ej} (in m^2) is the extinction cross-section corresponding to the j^{th} hydrometeor type. Size distributions are already available from Meso-NH: they are expressed as generalized gamma distributions, and depend on D and hydrometeor mass contents.

To compute backscattering and extinction cross-sections, a number of methods is available from literature. They range from the simplest one (e.g. Rayleigh) to very accurate methods that take into account the shape, size distribution of the scatterers (e.g. volumic methods). The Rayleigh approximation is valid when the size parameter (subsequently denoted by x) of the scatterers is well beyond unity. At C band the approximation is not well fulfilled and it is useful to compare results with more accurate methods. The Mie (or Lorenz-Mie) method consists in explicitely solving Maxwell's equations for an isotropic, homogeneous sphere. This method is therefore valid for any size parameter. However, it does not take the shape of scatterers into account. The Rayleigh-Gans approximation, which should not be confused with the Rayleigh-Debye approximation, consists in applying the Rayleigh approximation to spheroids, which are modeled as anisotropic spheres. Raindrops are modeled as spheroids the axis ratios of which are expressed as linear functions (e.g. Pruppacher and Beard, 1970) or more accurate polynomials (e.g. Andsager et al., 1999) of the equivolumic drop diameter. The T-matrix method can be viewed as a further refinement of the previous method which is valid for any body shape. However it is easier to implement for bodies of revolution (e.g. spheroids). It is then possible to study the influence of oblateness, size parameter, and canting on simulated reflectivities. The implementation of the Mie method resorts to the algorithm of Bohren and Huffman (1983) while the T-matrix one is based on the code developed by Mishchenko and Travis (1998).

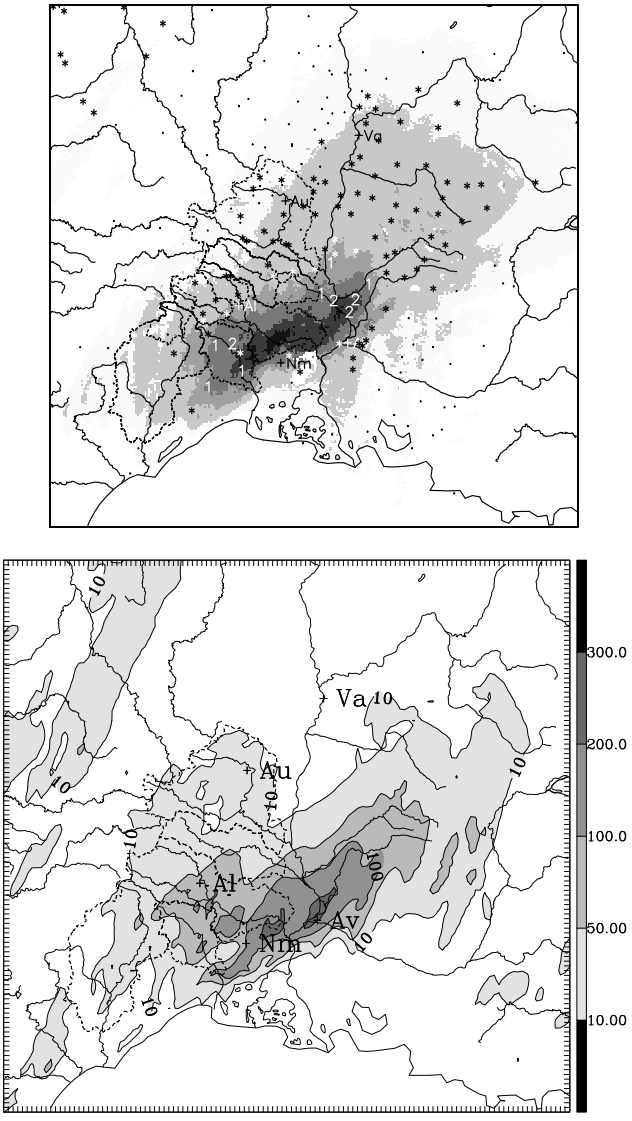

Fig. 1. (a) Observed from radar, and (b) simulated precipitations (in mm) between 12 and 22 UTC on 8 September 2002.

Scattering methods need a dielectric function, also called permittivity, to characterize the scatterers. For pure water particles, the dielectric function is taken from Liebe et al. (1991), while the model of Hufford (1991) is taken for pure ice. Melting graupeln are considered as randomly oriented ice spheroids embedded in a water matrix. The corresponding dielectric function is then computed following Bohren and Battan (1982).

Attenuation can be directly computed along with backscattering. Though attenuation may be neglected at S band, it can attain significant values at C band.

3 Case study

On 8–9 September 2002, a quasi-stationary mesoscale convective system has been standing over the same area in south-eastern France for more than 16 hours. This led to an extreme

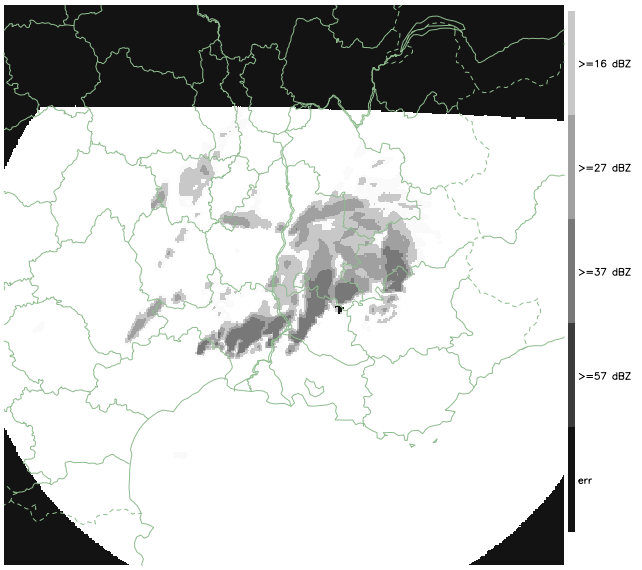

Fig. 2. Simulated reflectivities (E0 at 1.2 °) in dBZ at 21 UTC 8 September 2002. Pixels outside domain, underground, or out of radar range are black.

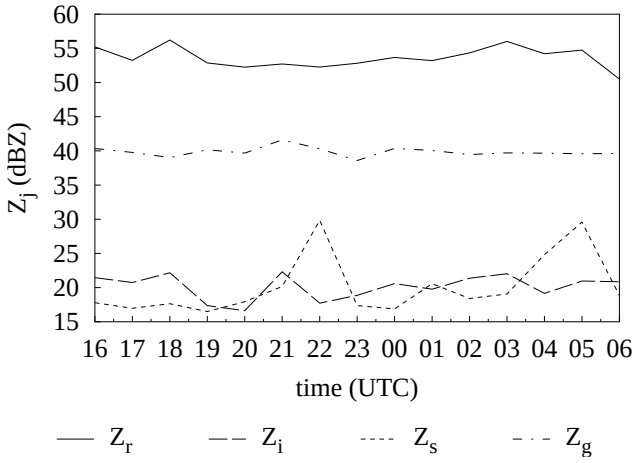

Fig. 3. Evolution of maximum reflectivities due to each hydrometeor type (in dBZ) between 16 UTC 8 September 2002 and 6 UTC 9 September 2002 (experiment E0).

flash-flood which entailed more than 20 casualties and a 1.2 billion euro economic damage. In 24 hours, the total precipitation amount has reached 691 mm. A detailed description of the meteorological situation is provided by Delrieu et al. (2004).

In order to image the results of the radar simulator, a simulation has been conducted with the anelastic non-hydrostatic Meso-NH model on this case. It has been run over two nested grids with horizontal resolutions of 9.5 km and 2.4 km respectively. The initial state is provided by the mesoscale initialization of Ducrocq et al. (2000) which is applied to a background large scale ARPEGE analysis valid for 12 UTC 8 September 2002. This fine scale initialization is composed of two steps: the first one consists of a mesoscale surface observation analysis. The second step of the fine scale initialization procedure consists of an ajustment of humidity and hydrometeors based on a pre-analysis of the cloudy and rainy areas associated with the developing storm of 8 September at 12 UTC. This pre-analysis is derived from radar reflectivities and from the IR METEOSAT brightness temperature. Ducrocq et al. (2002) have applied such a fine scale initialization to four convective cases that were characterized by weak synoptic forcing. They showed that the fine scale initialization procedure improved significantly the Quantitative Precipitation Forecast (QPF). This is also the case for the 8–9 September flash-flood (Ducrocq et al., 2004, and Fig. 1).

The Meso-NH model succeeds in simulating a quasi-stationary convective system, with both a convective and a stratiform part. That allows the radar simulator to sample different distributions of hydrometeors that are representative of deep convection situations.

Table 1. Experiments used to specify the observation operator.

Experiment	beam bending	scattering model	attenuation
E0	$4a/3$	Rayleigh	no
E1	local $\mathrm{d}n/\mathrm{d}z$	Rayleigh	no
E2	$4a/3$	Mie (C-band)	no
E3	$4a/3$	T-matrix (C-band)	no

4 Specifications of the observation operator

The strategy for specifying the observation operator mainly consists in assessing contributions of the different simulator modules to the overall synthetic reflectivity error. This being done, we are able to choose a particular implementation for each physical process, which is the result of a compromise between numerical accuracy, calculation cost, and feasibility. The accuracy of measured reflectivities is not expected to be below 1 dB. The sum of the errors associated to each simulator module should therefore be of the same order. In practise, much of these errors are independent, just as modules are independent, and we will only make sure that maximum errors in each module do not exceed a few dB and that the average error is sufficiently small. When these conditions are not met, a pre-processing scheme has to be found to flag gates that are prone to large errors.

A particular configuration, named E0, is being used as a reference. E0 uses an effective Earths's radius bending, Rayleigh scattering, neglects attenuation and no angular discretization is considered (each gate reflectivity is evaluated at only one point: the middle of the gate). Sensitivity tests are carried out by running other configurations that differ from the reference by only one module implementation (Table 1). Results are then compared to the reference in order to assess the effects of this change.

A sample of simulation E0 is given in Fig. 2.

In experiment E0, equivalent reflectivity factors rise up to 56 dBZ (Fig. 3). This value is mainly due to rain, and corresponds to a water content of 6.2 g m^{-3}. Reflectivities due to graupel attain 42 dBZ, which corresponds to a content of 5.1 g m^{-3}. Maximum reflectivities due to pure ice hydrometeors do not attain such values: snow can lead to associated reflectivities of 30 dBZ ($\rho_d r_s = 1.6\,\mathrm{g\,m^{-3}}$), while pristine ice can be responsible for reflectivities of 22 dBZ, which corresponds to $\rho_d r_i = 0.63\,\mathrm{g\,m^{-3}}$.

4.1 Beam shape

Taking into account the horizontal resolution of AROME, which will be of about 2 km, it does not seem necessary to use any quadrature technique to model the beam shape horizontally. However, vertically, the AROME resolution will be of the order of some 100 meters for lower levels, which will require an angular discretization of the beam if one wants to account for vertical heterogeneities in model fields. Some experiments have been carried out to determine the optimal number of points for the quadrature.

4.2 Beam bending

Experiment E1 does not differ very much from E0. A density current increases bending; it only widens ground echo areas at low elevations.

4.3 Scattering

Fig. 4a and b depict differences of equivalent reflectivity factors versus water content between some scattering theories and the approximation of Rayleigh for small spheres. Increasing the water content results in shifting the maximum of the raindrop size distribution towards large diameters, which increases the contribution of larger raindrops to the overall reflectivity. Approximations used in the different scattering methods depart from each other mainly for large raindrops (i.e., for large size parameters). This feature can be quantitatively assessed on Fig. 4a and b.

Differences in reflectivities due to rain between E2 and E0 do not exceed about 1 dB for water contents equal to about 6 g m^{-3}. Concerning raindrop oblateness, our results show that differences in rain-induced reflectivities between E3 and E0 can attain about 2.5 dB for water contents of 6 g m^{-3}. These results are corroborated by Figs. 4a and b.

Attenuation is caused by both air and hydrometeors. Air is usually said to occasion a two-way specific attenuation A of about 0.016 dB km^{-1} at C band, and about 0.004 dB km^{-1} at S band (e.g. Bean and Dutton, 1968).

It is well-known that discrepancies between Rayleigh and Mie calculations for attenuation efficiencies are worse than for backscattering efficiencies (see e.g. Gunn and East, 1954). It is still interesting to assess the effect of the Rayleigh approximation when accounting for size distributions. In Eq. (3), the extinction cross-section can be expressed as a series of powers of x. Usually, this series is only expanded

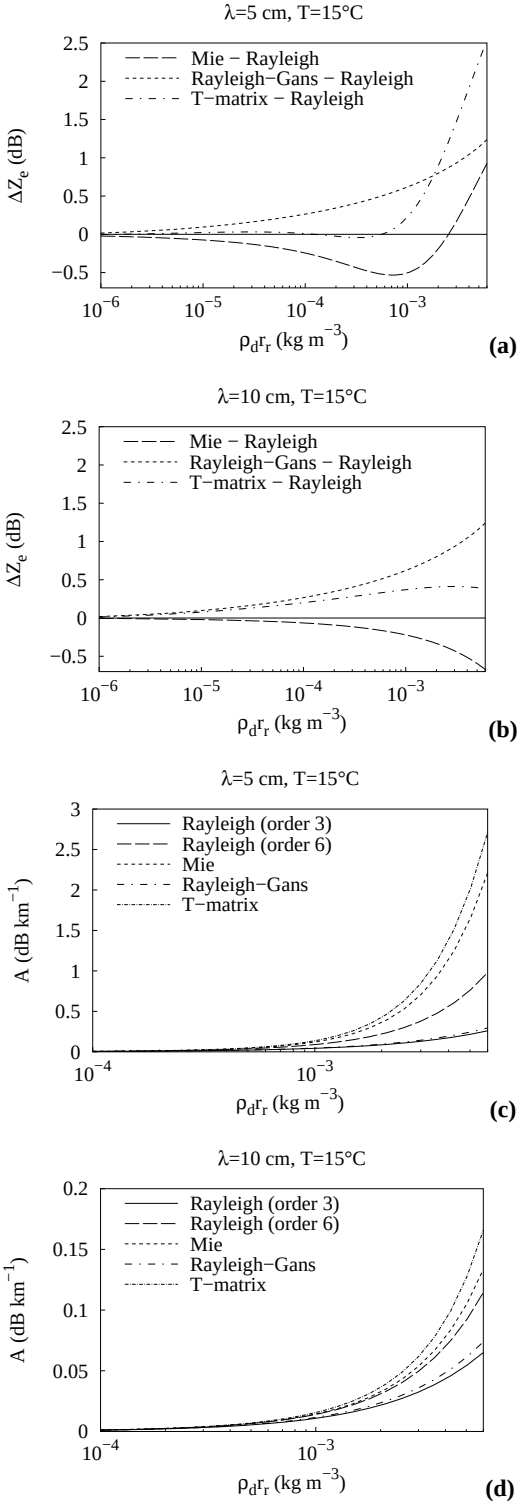

Fig. 4. Deviations from Rayleigh scattering by raindrops in terms of equivalent reflectivity factors as functions of water content: (a) $\lambda = 5$ cm and (b) $\lambda = 10$ cm, and two-way specific attenuations by rain as functions of water content: (c) $\lambda = 5$ cm and (d) $\lambda = 10$ cm, at 15°C. Rayleigh and Mie solutions concern spheres whereas Rayleigh-Gans and T-matrix ones are computed for spheroids with axis ratios that follow Pruppacher and Beard (1970). Note that A scales differ in (c) and (d).

up to the term in x^3. Fig. 4c and d show specific attenuation due to rain for different scattering models. It is clear on this figure that truncating the expression of specific attenuation under the Rayleigh approximation to order 3 in x is not satisfactory. This effect is due to the particular dielectric function of water. Indeed, the truncation to order 3 is only valid if

$$x \ll \left(\frac{3\Im(K_w)}{2\Re(K_w^2)} \right)^{\frac{1}{3}} . \quad (4)$$

where $\Re$ and $\Im$ denote the real and imaginary parts of their argument, respectively. At 15°C and $\lambda = 5$ cm, it means that D should be well beyond 4.4 mm, which is clearly not the case for higher water contents. The Rayleigh-Gans approach also provides an expression of A that is limited to the 3rd order, which explains why its curve is not far away from the 3rd order Rayleigh one. If the Rayleigh approximation up to 6th order approaches the Mie solution, at $\lambda = 5$ cm it is still far from the Mie reference. As for reflectivities, raindrop oblateness enhances horizontal specific attenuation. It can be quantified by comparing the T-matrix solution to the Mie one on Fig. 4c and d. Our results at C- and S-bands on the 8 September 2002-case show that the Rayleigh approximation cannot be used to compute attenuations because it leads to large errors.

Eq. (2) involves two improper integrals over D. These integrations are carried out within one single loop by means of a Gauss-Laguerre quadrature. For Rayleigh scattering, Gauss-Laguerre quadrature gives exact results if the number of points is at least 4. It means that we have to take at least 4 points for other methods. Sensitivity experiments of Mie computations involving our case study show that taking 5 points leads to an average error of 0.03 dB, and that all errors remain below 1 dB.

5 Conclusions

A modular simulator for radar reflectivities was developed in the diagnostic part of Meso-NH. Each module, which represents a particular physical process, received a number of different implementations. These implementations differ in their complexity, accuracy and CPU time consumption. It allowed us to find an optimal combination for an observation operator that fulfills the following conditions: the forward operator gives sufficiently accurate results compared to measurement errors, its implementation in a parallel code is feasible, and it does not require too much computer time and memory. For instance, the need for a parallel code makes it difficult to use gate-by-gate computations that are necessary for beam bending computations that use local air refractive index gradients, or for attenuation because it needs all reflectivities previously computed on the beam. Therefore, the effective Earth's radius model will be used for beam bending computations. Abnormal propagation situations will therefore have to be handled before inclusion of the data in the assimilation scheme. Quality control checks during data acquisition are expected to be able to detect most of the radars that undergo subrefractions. Just as for beam bending, we cannot afford attenuation computations in a parallel code. This issue has therefore to be treated before the use of radar data by the assimilation process. In consequence, regions beyond high reflectivity cores on radar images will be flagged. However, attenuation will be anyway implemented for monitoring purposes. Concerning beam ray discretization, one angle horizontally and 3 angles vertically should meet the requirements. Rayleigh scattering is sufficient to simulate reflectivities. Other solutions are too expensive (T-matrix), or do not yield consequent improvements (Mie). However, if one wants to compute attenuation, it will be necessary to use at least Mie theory.

As a by-product, this radar simulator enables comparisons of model outputs to radar observations. It is also a good basis for easily implementing polarimetric products or Doppler radial winds.

References

Alberoni, P. P., Ducrocq, V., Gregorič, G., Haase, G., Holleman, I., Lindskog, M., Macpherson, B., Nuret, M., and Rossa, A.: Quality and Assimilation of Radar Data for NWP – A Review, Tech. rep., EUR 20600 – COST Action 717, 2003.

Anagnostou, E. N. and Krajewski, W. F.: Simulation of radar reflectivity fields: Algorithm formulation and evaluation, Water Resour. Res., 33, 1419–1428, 1997.

Andsager, K., Beard, K. V., and Laird, N. F.: Laboratory measurements of axis ratios for large raindrops, J. Atmos. Sci., 56, 2673–2683, 1999.

Bean, B. R. and Dutton, E. J.: Radio meteorology, Dover, New York, 1968.

Bohren, C. F. and Battan, L. J.: Radar backscattering of microwaves by spongy ice spheres, J. Atmos. Sci., 39, 2623–2628, 1982.

Bohren, C. F. and Huffman, D. R.: Absorption and Scattering of Light by Small Particles, John Wiley & Sons, 1983.

Boudevillain, Br. and Andrieu, H.: Assessment of vertically integrated liquid (VIL) water content radar measurement, J. Atmos. Oceanic Technol., 20, 807–819, 2003.

Caniaux, G., Redelsperger, J.-L., and Lafore, J.-Ph.: A numerical study of the stratiform region of a fast-moving squall line, J. Atmos. Sci., 51, 2046–2074, 1994.

Capsoni, C., D'Amico, M., and Nebuloni, R.: A multiparameter polarimetric radar simulator, J. Atmos. Oceanic Technol., 18, 1799–1809, 2001.

Clark, T. L. and Farley, R. D.: Severe downslope windstorm calculations in two and three spatial dimensions using anelastic interactive grid nesting: A possible mechanism for gustiness, J. Atmos. Sci., 41, 329–350, 1984.

Delrieu, G., Ducrocq, V., Gaume, É., Nicol, J., Payrastre, O., Yates, E., Andrieu, H., Ayral, P.-A., Bouvier, Chr., Creutin, J.-D., Livet, M., Anquetin, S., Lang, M., Neppel, L., Obled, Ch., Parent du Châtelet, J., Saulnier, G.-M., Walpersdorf, A., and Wobrock, W.: The catastrophic flash-flood event of 8–9 September 2002 in the Gard region, France: a first case study for the Cévennes-Vivarais Mediterranean Hydro-meteorological Observatory, J. Hydrometeor., accepted, 2004.

Doviak, R. J. and Zrnić, D. S.: Doppler Radar and Weather Observations, Academic Press, San Diego, California, 2nd edn., 1993.

Ducrocq, V., Lafore, J.-Ph., Redelsperger, J.-L., and Orain, Fr.: Initialization of a fine scale model for convective system prediction: A case study, Quart. J. Roy. Meteor. Soc., 126, 3041–3066, 2000.

Ducrocq, V., Ricard, D., Lafore, J.-Ph., and Orain,Fr.: Storm-scale numerical rainfall prediction for five precipitating events over France: On the importance of the initial humidity field, Wea. Forecasting, 17, 1236–1256, 2002.

Ducrocq, V., Lebeaupin, C., Thouvenin, Th., Giordani, H., Chancibault, K., Anquetin, S., and Saulnier, G.-M.: L'événement des 8–9 septembre 2002 : situation météorologique et simulation à mésoéchelle (The 8–9 September 2002 event: Meteorological situation and mesoscale simulation), in Colloque "Crues méditerranéennes", Société Hydrotechnique de France, Nîmes, France, 2004.

Giuli, D., Baldini, L., and Facheris, L.: Simulation and modeling of rainfall radar measurements for hydrological applications, Natural Hazards, 9, 109–122, 1994.

Gunn, K. L. S. and East, T. W. R.: The microwave properties of precipitation particles, Quart. J. Roy. Meteor. Soc., 80, 522–545, 1954.

Haase, G. and Crewell, S.: Simulation of radar reflectivities using a mesoscale weather forecast model, Water Resour. Res., 38, 2221–2231, 2000.

Hufford, G. A.: A model for the complex permittivity of ice at frequencies below 1 THz, Int. J. Infrar. Millim. Waves, 12, 677–682, 1991.

Lafore, J.-Ph., Stein, J., Asencio, N., Bougeault, Ph., Ducrocq, V., Duron, J., Fischer, C., Héreil, Ph., Mascart, P., Masson, V., Pinty, J.-P., Redelsperger, J.-L., Richard, É., and Vilà-Guerau de Arellano, J.: The Meso-NH Atmospheric Simulation System. Part I: Adiabatic formulation and control simulations. Scientific objectives and experimental design, Ann. Geophys., 16, 90–109, 1998.

Liebe, H. J., Hufford, G. A., and Manabe, T.: A model for the complex permittivity of water at frequencies below 1 THz, Int. J. Infrar. Millim. Waves, 12, 659–674, 1991.

Lindskog, M., Salonen, K., Järvinen, H., and Michelson, D. B.: Doppler Radar Wind Data Assimilation with HIRLAM 3DVAR, Mon. Wea. Rev., 132, 1081–1092, 2004.

Mishchenko, M. I. and Travis, L. D.: Capabilities and limitations of a current Fortran implementation of the T-matrix method for randomly oriented, rotationally symmetric scatterers, J. Quant. Spectrosc. Radiat. Transfer, 60, 309–324, 1998.

Pellarin, Th., Delrieu, G., Saulnier, G.-M., Andrieu, H., Vignal, B., and Creutin, J.-D.: Hydrologic visibility of weather radar systems operating in mountainous regions: case study for the Ardèche catchment (France), J. Hydrometeor., 3, 539–555, 2002.

Pinty, J.-P. and Jabouille, P.: A mixed-phase cloud parameterization for use in a mesoscale non-hydrostatic model: Simulations of a squall line of orographic precipitation, in Preprints of Conf. on Cloud Physics, pp. 217–220, Amer. Meteor. Soc., Everett, WA, 1998.

Probert-Jones, J. R.: The radar equation in meteorology, Quart. J. Roy. Meteor. Soc., 88, 485–495, 1962.

Pruppacher, H. R. and Beard, K. V.: A wind tunnel investigation of the internal circulation and shape of water drops falling at terminal velocity in air, Quart. J. Roy. Meteor. Soc., 96, 247–256, 1970.

Schelleng, J. C., Burrows, C. R., and Ferrell, E. B.: Ultra-short-wave propagation, Proc. IRE, 21, 427–463, 1933.

Smith, Jr., E. K. and Weintraub, S.: The constants in the equation for atmospheric refractive index at radio frequencies, Proc. IRE, 41, 1035–1037, 1953.

Stein, J., Richard, É., Lafore, J.- Ph., Pinty, J.-P., Asencio, N., and Cosma, S.: High-Resolution Non-Hydrostatic Simulations of Flash-Flood Episodes with Grid-Nesting and Ice-Phase Parameterization, Meteor. Atmos. Phys., 72, 203–221, 2000.

Vivekanandan, J., Raghavan, R., and Bringi, V. N.: Polarimetric radar modeling of mixtures of precipitation particles, IEEE Trans. Geosci. Remote Sens., 31, 1017–1030, 1993.

Wu, B., Verlinde, J., and Sun, J.: Dynamical and microphysical retrievals from Doppler radar observations of a deep convective cloud, J. Atmos. Sci., 57, 262–283, 2000.

Xiao, Q., Sun, J., Lee, W.-C., Lim, E., Guo, Y., Barker, D. M., and Kuo, Y.-H.: Assimilation of Doppler radar observations with a regional 3D-VAR system: A heavy rainfall case study, in Proc. 31st Conf. on Radar Meteorology, pp. 165–168, Amer. Meteor. Soc., Seattle, Washington, 2003.